# Figures and figure supplements

Insights from aquaporin structures into drug-resistant sleeping sickness

**Modestas Matusevicius, Robin A Corey and Marcos Gragera *et al*.**


**Figure 1.** Alignment of aquaporin amino acid sequences. Amino acid sequences of AQP2 and AQP3 from *Trypanosoma brucei brucei* (Tbb) are aligned with chimeric aquaporins from drug-resistant strains (P1000, 427MR, and R25) and a chimera from drug-resistant *T. b. gambiense* (TbgAQP2/3). Three identical sequences are shown of TbbAQP2 with residues making contact to either glycerol, pentamidine, or melarsoprol highlighted (cyan, green, or yellow, respectively). Red bars represent transmembrane regions. Residues highlighted in grey are conserved in all sequences. The conserved NSA/NPS motif in TbAQP2 and the analogous NPA/NPA motif in TbAQP3 are in purple font and the residues mutated for the molecular dynamics (MD) simulation

*Figure 1 continued on next page*

*Figure 1 continued*

studies (I110W, L258Y, and L264R) are in red. Sequence information was obtained from ***Munday et al., 2014*** except R25 (***Unciti-Broceta et al., 2015***) and TbgAQP2/3 (678–800) (***Pyana Pati et al., 2014***).

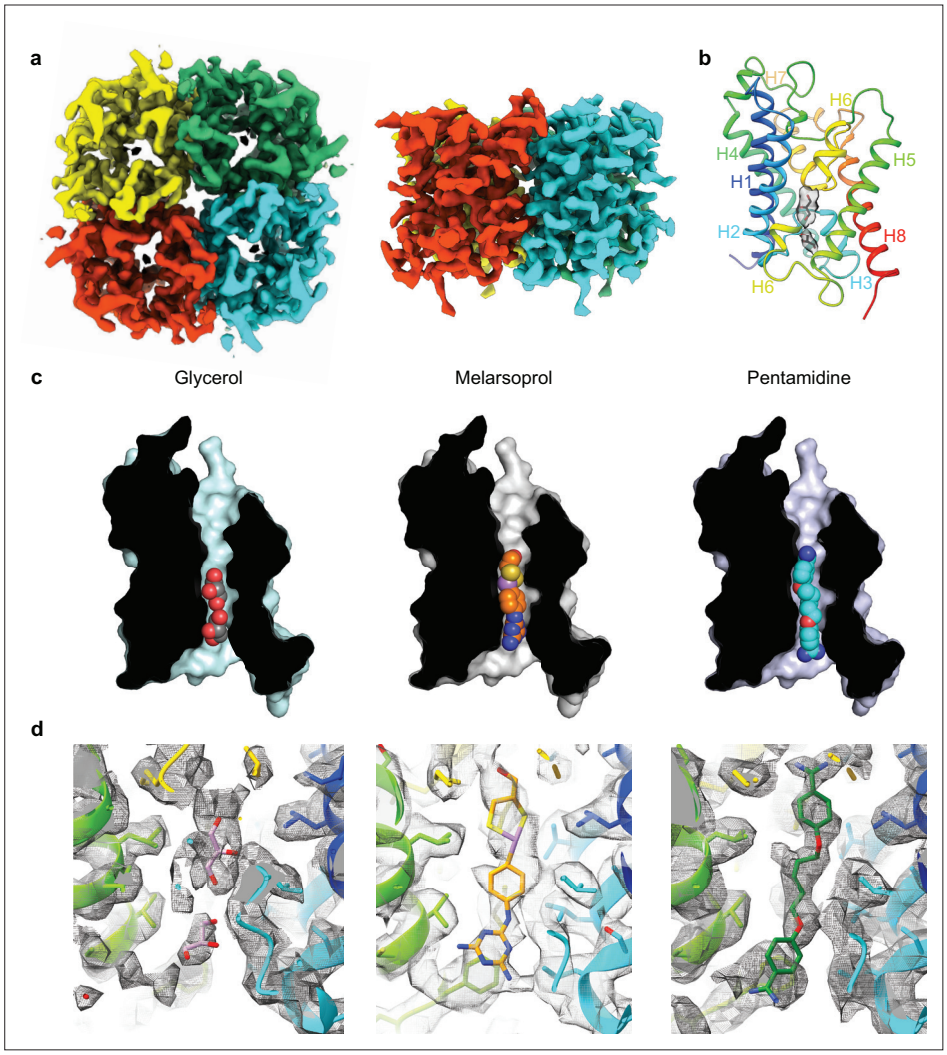


**Figure 2.** Cryo-EM structures of TbAQP2 bound to either glycerol, melarsoprol, or pentamidine. (**a**) Overall structure of the TbAQP2 tetramer viewed either from the extracellular surface or within the membrane plane. (**b**) Structure of protomer A of TbAQP2 viewed as a cartoon (rainbow colouration) with glycerol (sticks) bound. The cryo-EM density for glycerol is shown as a grey surface. (**c**) Cut-away views of the channel in each of the TbAQP2 structures showing bound substrates and drugs (spheres) with atoms coloured according to type: red, oxygen; yellow, sulphur; blue, nitrogen; purple, arsenic; carbon, grey (glycerol), orange (melarsoprol), or cyan (pentamidine). (**d**) Cryo-EM densities (grey surface) for glycerol, melarsoprol, and pentamidine in their respective structures. See ***Figure 2—figure supplements 6 and 7*** for different views of the substrates and comparisons between densities.

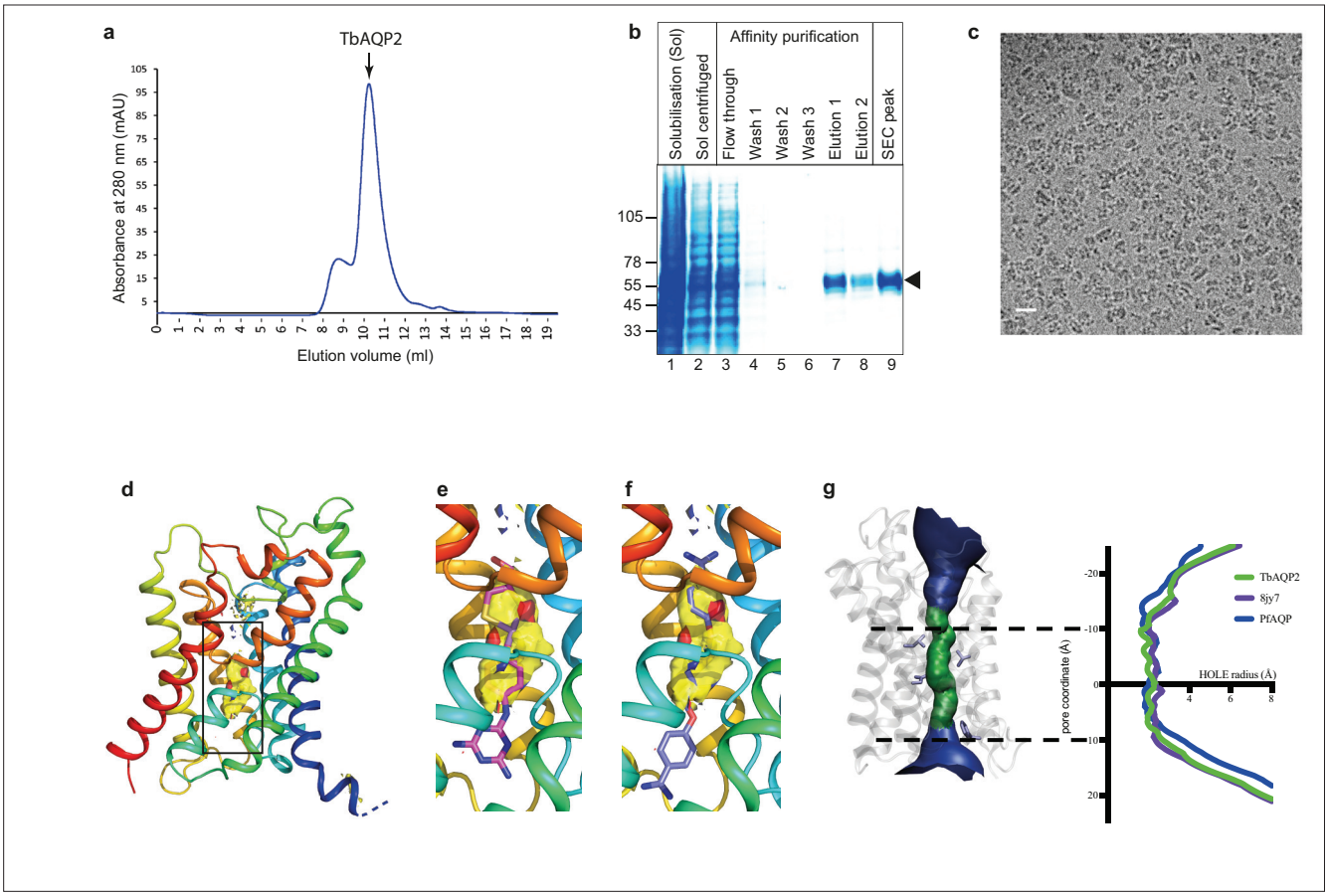


**Figure 2—figure supplement 1.** Purification of TbAQP2 and identification of the drug binding site by hotspot analysis. (**a**) Size exclusion chromatography (SEC) trace of affinity purified TbAQP2. (**b**) Coomassie-stained SDS–PAGE gel of fractions during detergent solubilisation (Sol), $Ni^{2+}$-affinity chromatography and from the SEC column. (**c**) Cryo-EM electron micrograph showing the particle distribution of TbAQP2 (scale bar 100 Å). (**d**) A region of TbAQP2 that was identified as being most likely to bind a ligand is shown (yellow surface) and is mapped on to the structure of TbAQP2 determined here in rainbow colouration. (**e**) As in (**d**) but also containing pentamidine (cyan sticks). (**f**) HOLE (***Smart et al., 1993***) trace for our resolved TbAQP2 structure, compared to a previously released TbAQP2 structure (8yj7) (***Chen et al., 2024***) and *Plasmodium falciparum* AQP (***Newby et al., 2008***).

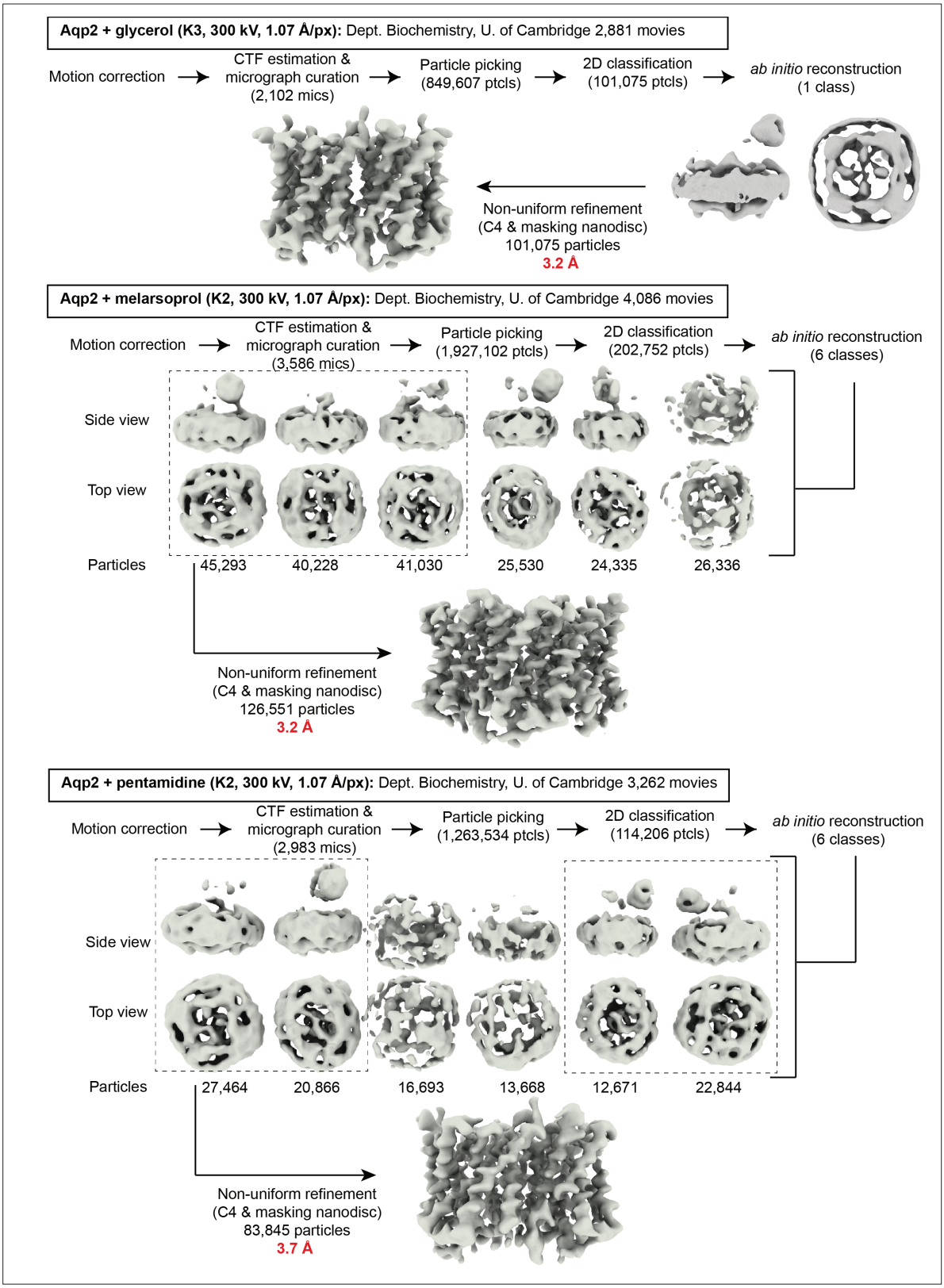


**Figure 2—figure supplement 2.** Flow chart of the cryo-EM image processing and structure determination. See the Methods section for the computer programmes used for each step and for further details.

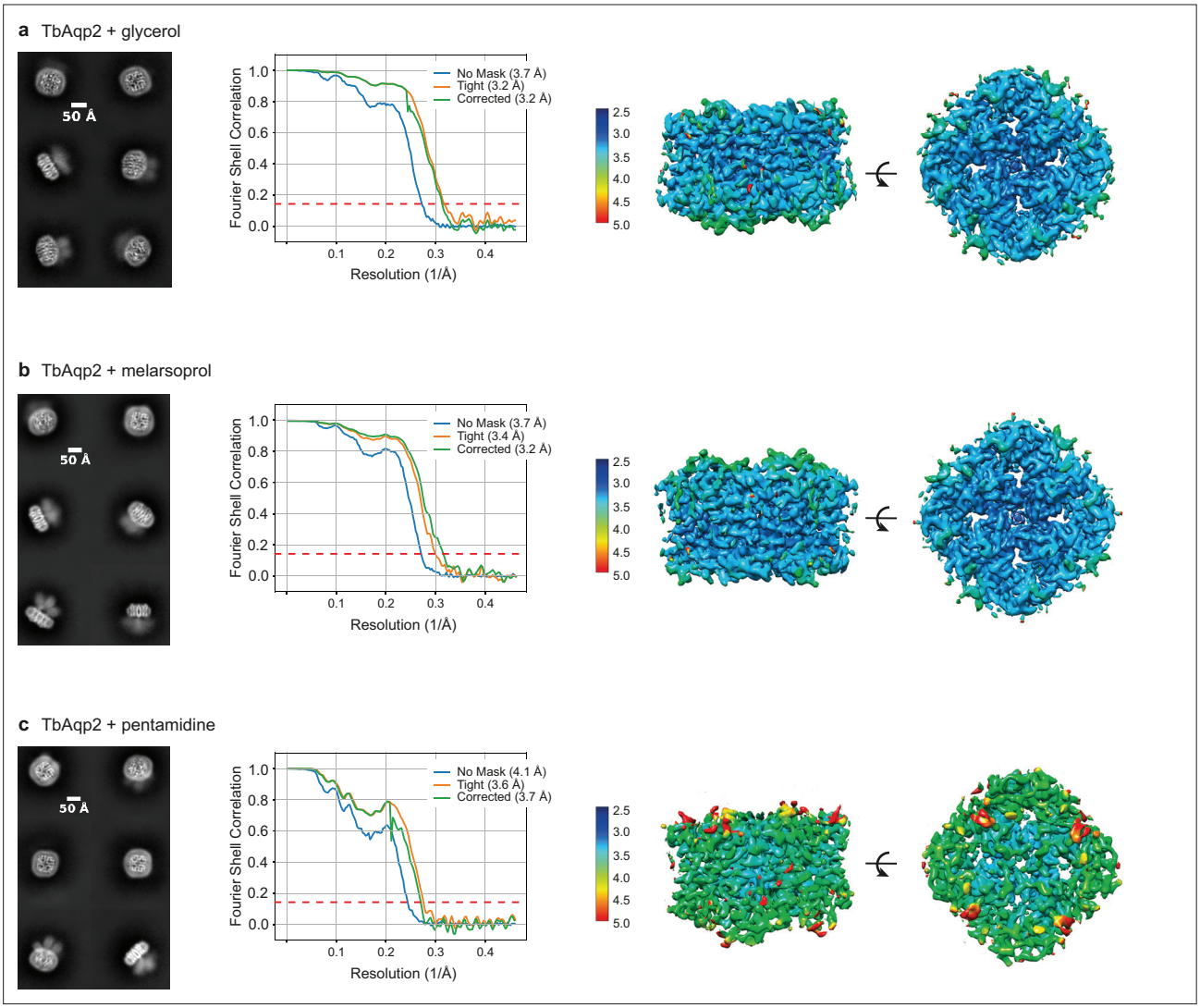


**Figure 2—figure supplement 3.** Local resolution maps of TbAQP2 structures. (**a–c**) 2D class averages for each of the structures (left panels), FSC curves of the reconstructions with estimates for resolution determined using an FSC of 0.143 as implemented in cryoSPARC (middle panels) and local resolution estimations as calculated by MonoRes (right panels).

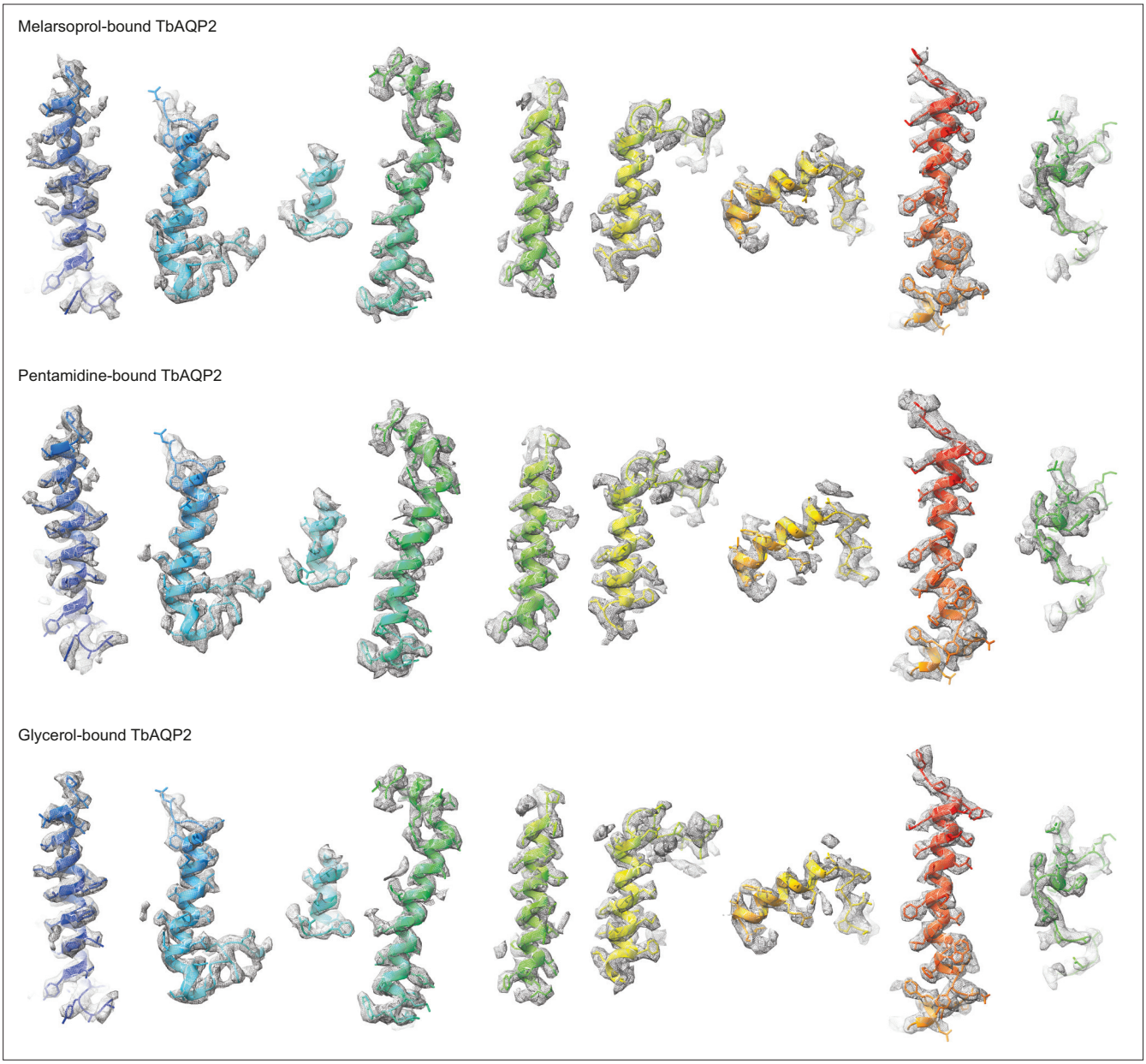


**Figure 2—figure supplement 4.** Density maps of secondary structure elements in the TbAQP2 structures. Colouring is the same as in ***Figure 1b***.

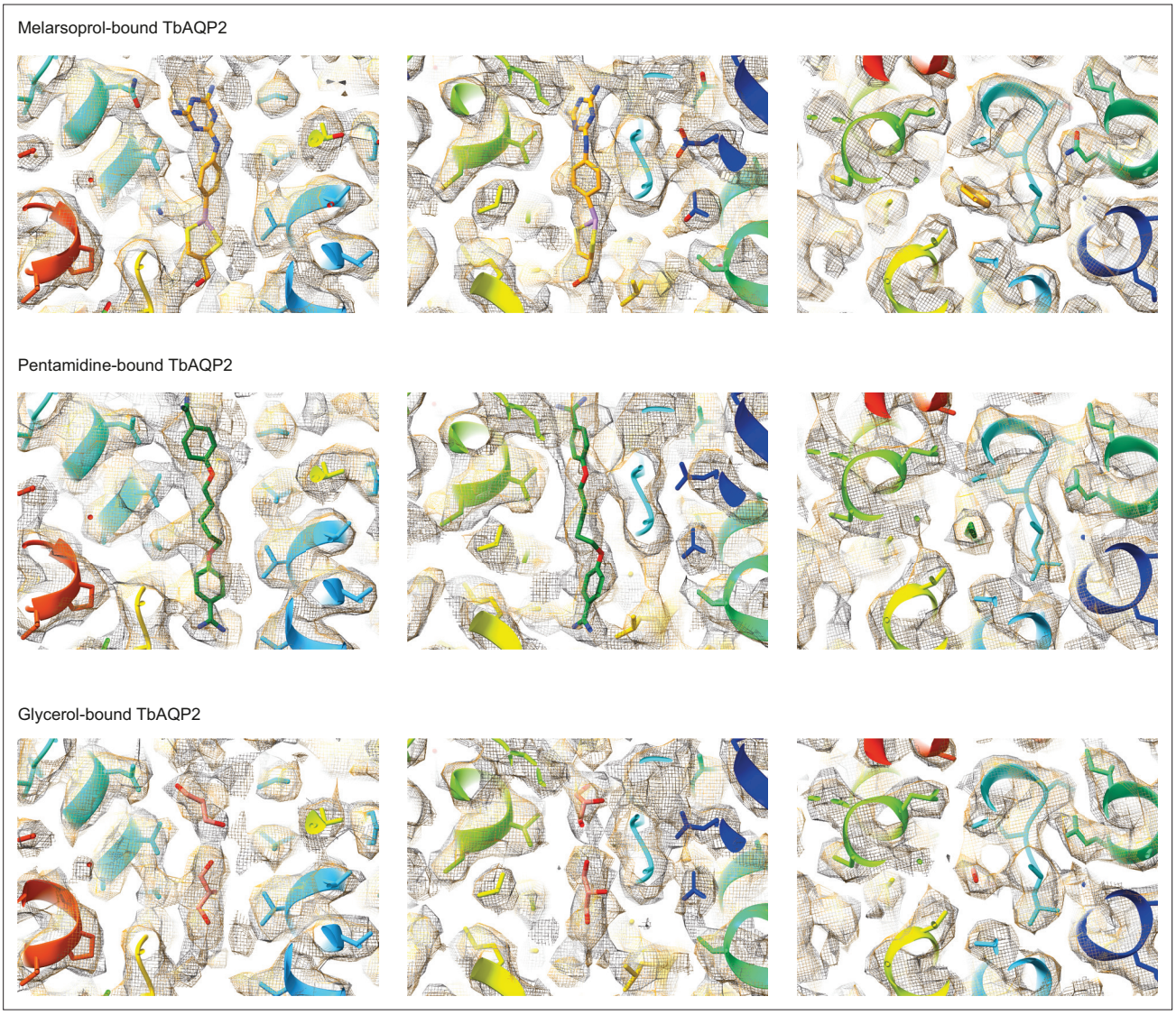


**Figure 2—figure supplement 5.** Density half maps of ligands bound in the TbAQP2 structures.

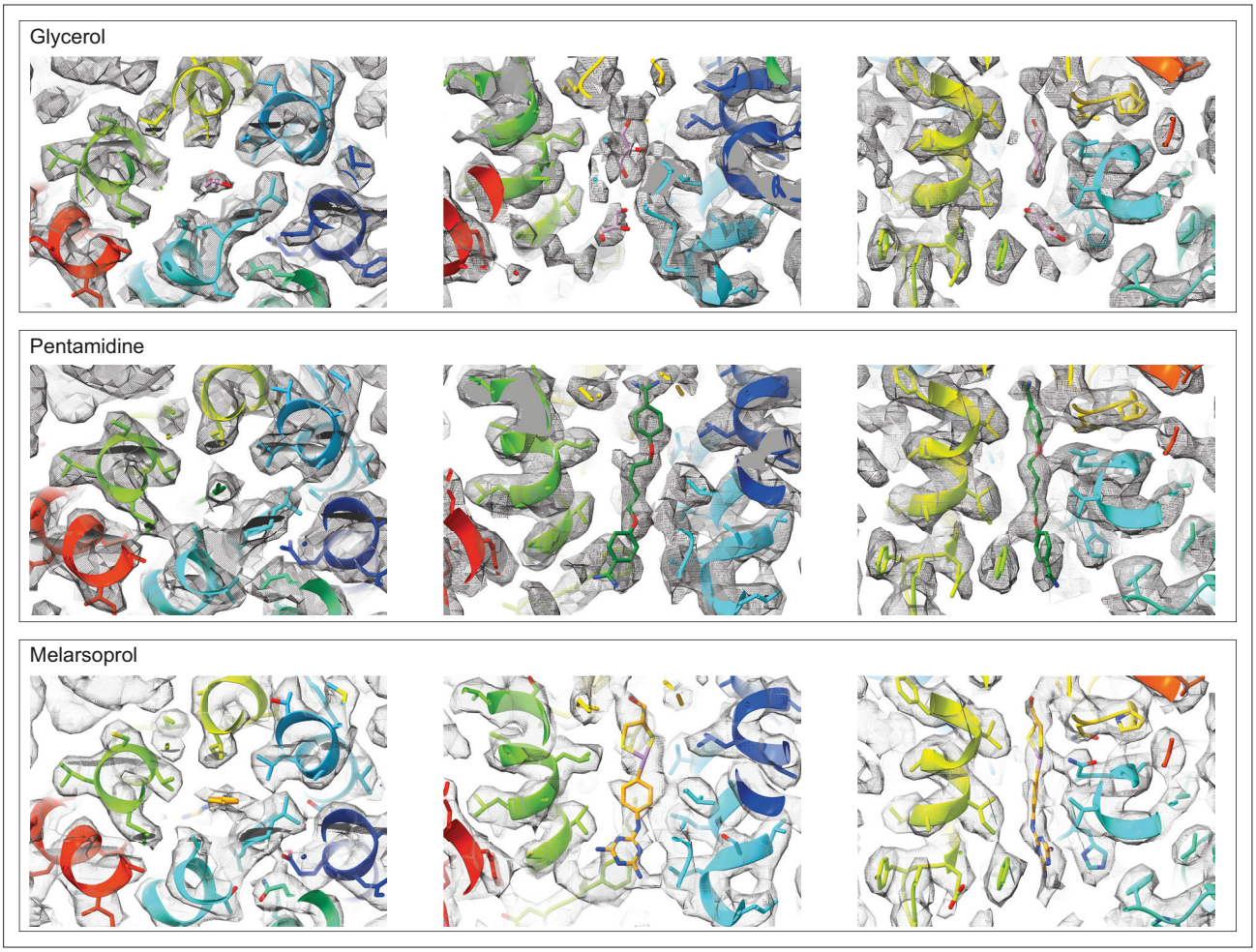


**Figure 2—figure supplement 6.** Depictions of the side chain and substrate densities.

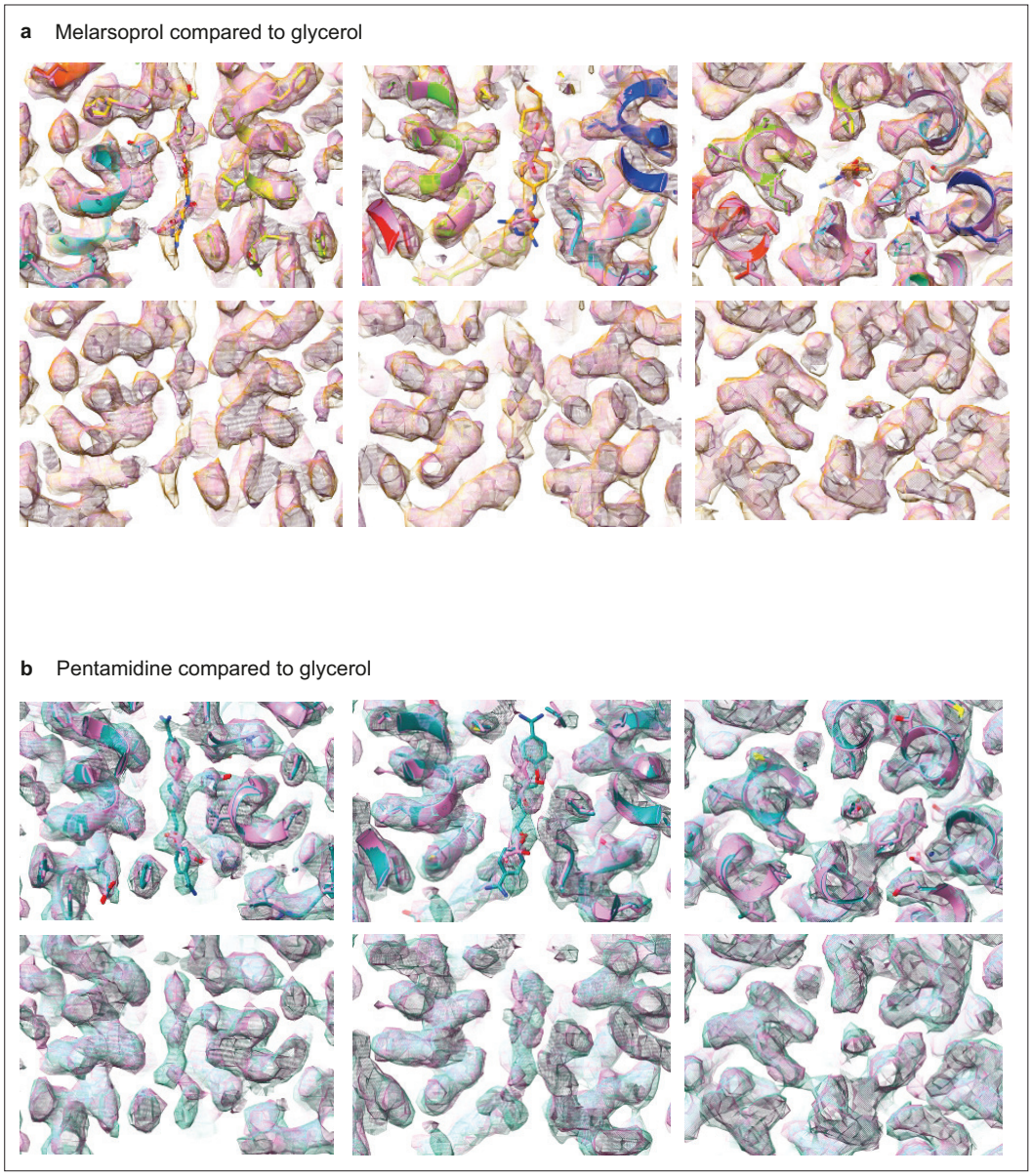


**Figure 2—figure supplement 7.** Comparisons between substrate densities. (**a**) Comparison between melarsoprol and glycerol. (**b**) Comparison between pentamidine and glycerol.

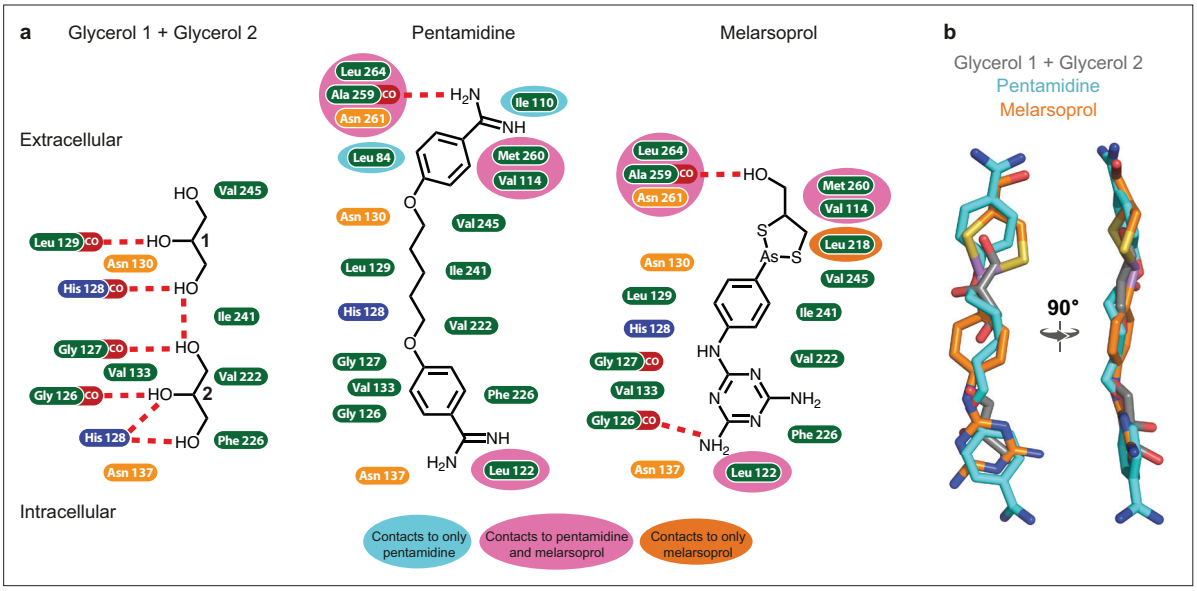


**Figure 3.** Interactions between TbAQP2 and bound substrates and drugs. (**a**) Amino acid residues containing atoms ≤3.9 Å from substrate or drug model in the cryo-EM structures are depicted and coloured according to the chemistry of the side chain: hydrophobic, green, positively charged, blue; polar, orange. Interactions with a backbone carbonyl group are shown as CO (red) and potential hydrogen bonds are shown as red dashed lines. Residues highlighted in an additional colour (grey, pale blue, pink, or dark orange) make contacts in two or less of the structures (as indicated on the figure), whilst those without additional highlighting make contacts in all three structures. (**b**) Protomer A from each structure was aligned and the positions of the two glycerol molecules (grey), melarsoprol (orange), and pentamidine (cyan) are depicted.

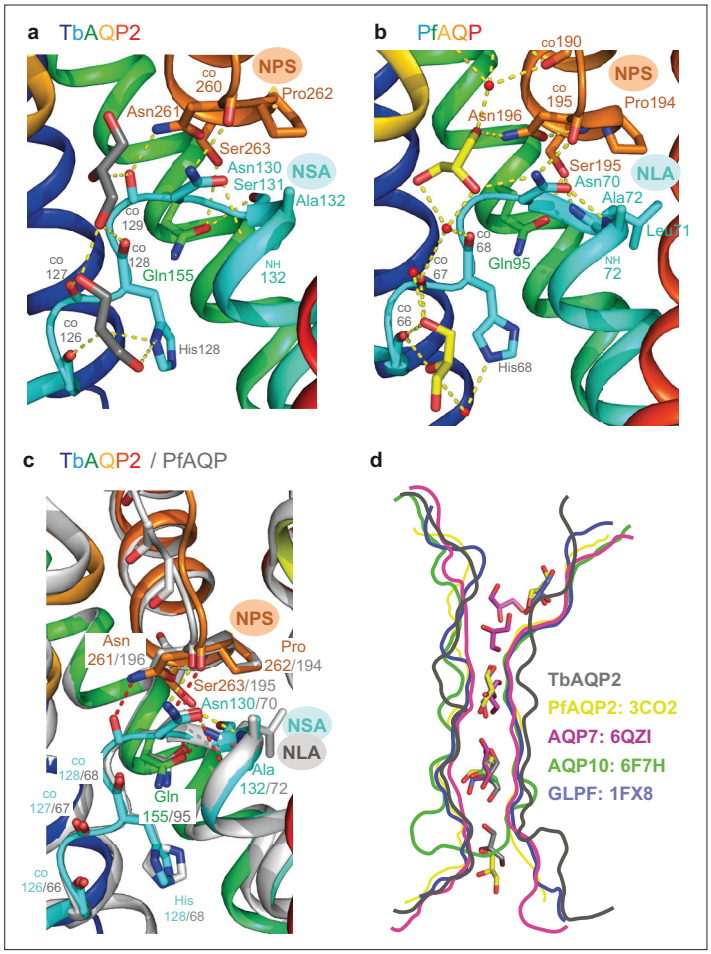


**Figure 4.** Comparison between conserved glycerol-binding regions of TbAQP2 and PfAQP. (**a**) The structure of TbAQP2 is depicted (rainbow colouration) with residues shown that make hydrogen bonds (yellow dashed lines) to either glycerol (grey) or in the NPS/NSA motifs. CO, backbone carbonyl groups involved in hydrogen bond formation. (**b**) The structure of PfAQP2 is depicted (rainbow colouration) with residues shown that make hydrogen bonds (yellow dashed lines) to either glycerol (yellow sticks) or water (red spheres), or in the NPS/NLA motifs. CO, backbone carbonyl groups involved in hydrogen bond formation. (**c**) Structures of TbAQP2 (rainbow colouration) and PfAQP are superimposed to highlight structural conservation of the NPS and NSA/NLA motifs. (**d**) Outline of channel cross-sections from aquaglyceroporins containing bound glycerol molecules (sticks): TbAQP2 (grey); PfAQP (yellow; PDB ID 3CO2); human AQP7 (magenta, PDB ID 6QZI); human AQP10 (green, PDB ID 6F7H); and *Escherichia coli* GlpF (purple, PDB ID 1*FX*8).

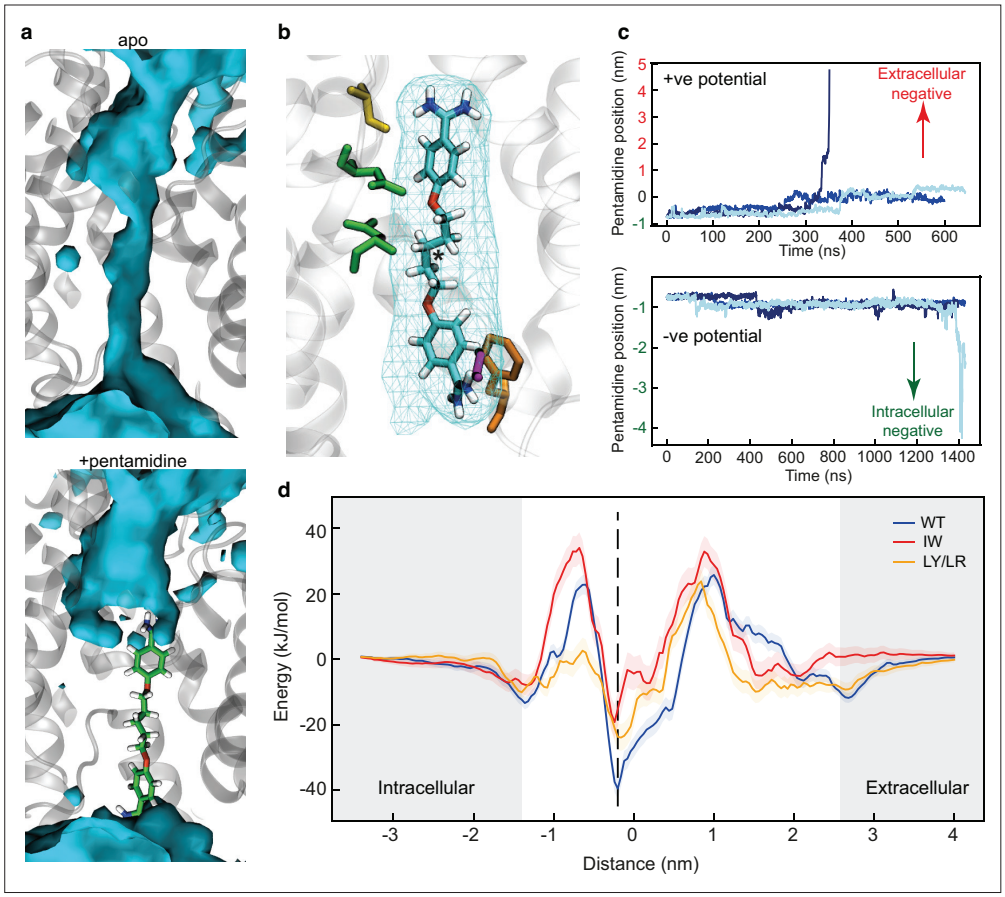


**Figure 5.** Molecular dynamics (MD) simulations of pentamidine-bound TbAQP2. (**a**) Density of water molecules (blue) through the TbAQP2 central cavity from MD. Bound pentamidine (sticks, green) abolishes the ability of TbAQP2 to transport water molecules. (**b**) View of pentamidine (cyan, carbon; red, oxygen; blue, nitrogen; white, hydrogen) bound to TbAQP2. Cyan mesh shows the density of the molecule across the MD simulation, and the asterisk shows the position of the centre of mass (COM). (**c**) Upon application of a membrane potential, the pentamidine position as defined by the COM moves along the *z*-dimension in relation to the COM of the channel, with three independent repeats shown in different shades of blue. The bottom graph is for the potential in the physiological direction (negative intracellular). (**d**) Energy landscapes for pentamidine through the TbAQP2 central cavity as calculated using umbrella sampling. Separate calculations were made for monomeric WT TbAQP2 and TbAQP2 with I110W (IW) or L258Y/L264R (LY/LR) mutations. Each trace is built from 167 × 40 ns windows, with the histogram overlap and convergence plotted in ***Figure 5—figure supplement 3a, b***. The position of the membrane phosphates is shown as grey bars, and the structural binding pose is shown as a dotted line.

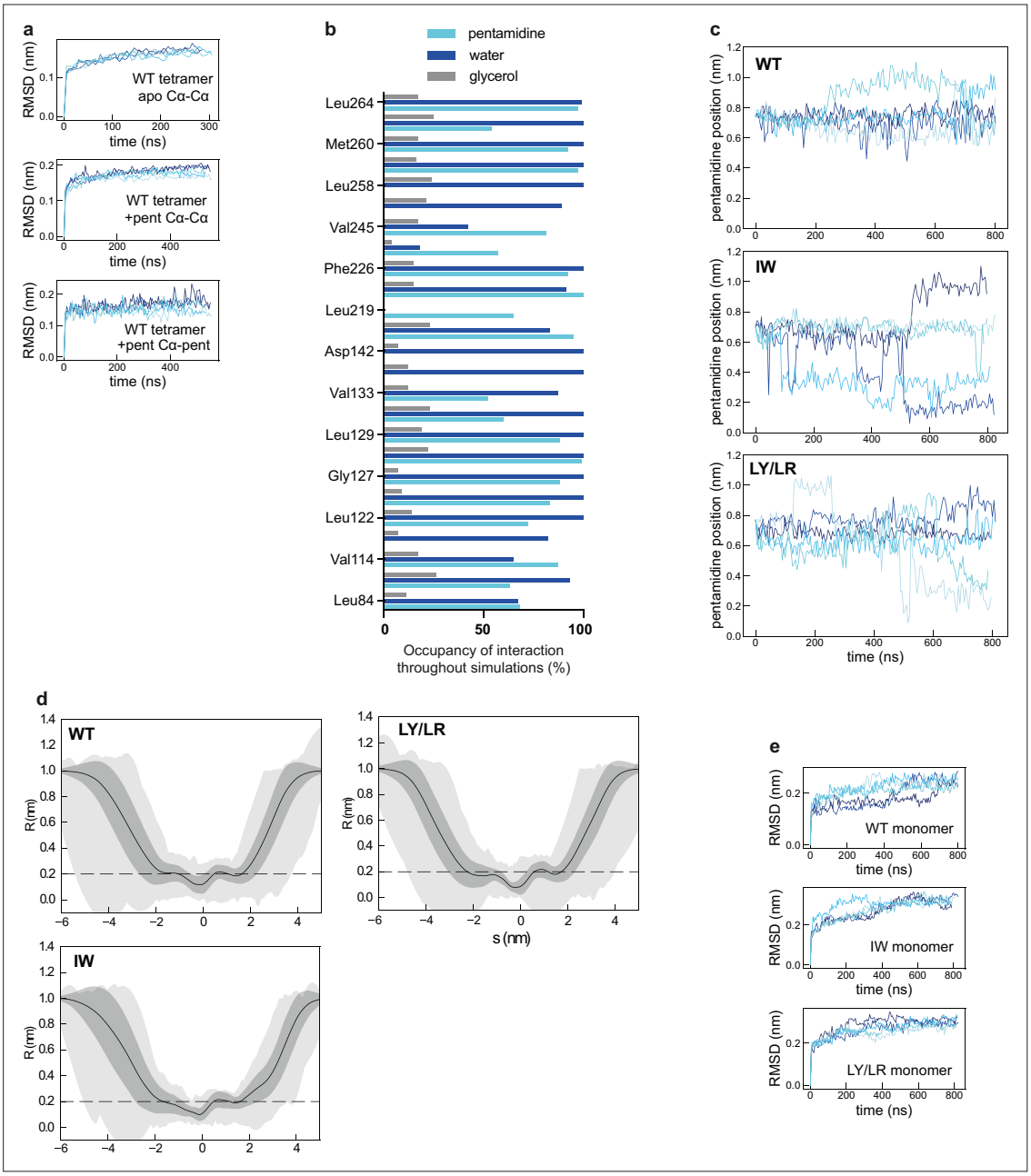


**Figure 5—figure supplement 1.** Molecular dynamics (MD) simulations. (**a**) RMSDs for simulations of tetrameric WT TbAQP2. Trajectories were fitted on the Cα atoms and RMSDs were calculated for either Cα atoms for apo TbAQP2 (top), Cα atoms for pentamidine (pent) bound TbAQP2 (middle), or for the pentamidine molecule itself, that is in relation to the Cα of the channel (bottom). Five independent repeats are shown as blue traces. (**b**) Percentage of time (occupancy) a given residue is within 3.9 Å of either pentamidine, water or glycerol during the MD simulations. (**c**) Plotting the *z*-axis position of pentamidine when bound to monomeric TbAQP2 in a WT, IW, or LY/LR background. (**d**) Pore radius profiles from simulations of apo monomeric WT, IW, or LY/LR TbAQP2. Analyses were run using the CHAP package (***Klesse et al., 2019***) with traces showing the mean (black line), standard deviation (dark grey), and range (light grey) for all frames over 5 × 800 ns of simulation. (**e**) As panel (**a**) but for Cα atoms from monomeric TbAQP2 in a WT background, or with I110W (IW) or L258Y/L264R (LY/LR) mutations.

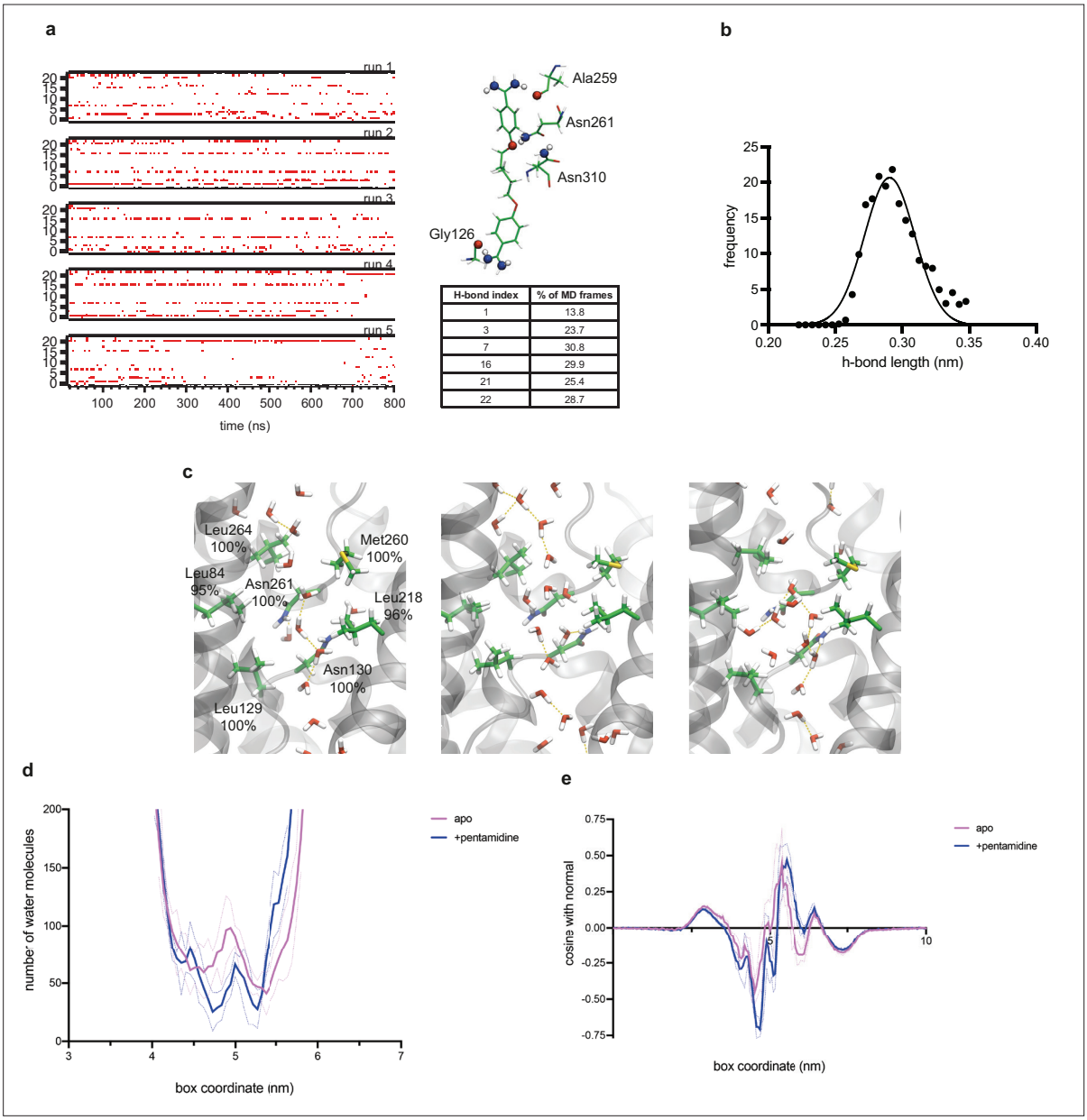


| H-bond index | % of MD frames |
|---|---|
| 1 | 13.8 |
| 3 | 23.7 |
| 7 | 30.8 |
| 16 | 29.9 |
| 21 | 25.4 |
| 22 | 28.7 |

**Figure 5—figure supplement 2.** Water in molecular dynamics (MD) simulations. (**a**) Hydrogen-bond analysis from *gmx hbond* between the pentamidine and channel. Across the 5 independent MD runs of the monomeric TbAQP2 MD simulations, 23 hydrogen bonds are formed, but only 6 appear to be high occupancy. These are highlighted on the image along with their index number, and their quantification is shown below. (**b**) Hydrogen-bond distances from the bonds in panel (**a**) plotted as a frequency plot. The average bond length was 0.29 ± 0.02 nm, suggesting moderate strength. (**c**) Snapshots from MD showing water progression through the TbAQP2 channel in the absence of pentamidine. Three snapshots are shown. Residues that form especially high contact with water molecules (values given in brackets) are highlighted in each snapshot. Water–water hydrogen bonds, as computed using VMD, are shown in yellow dashed lines. (**d**) Number of water molecules along the TbAQP2 channel ±pentamidine, as computed using *gmx h2order* on the monomeric TbAQP2 MD simulations. (**e**) Orientation of the waters in each of the slices along the channel, as computed using *gmx h2order*.

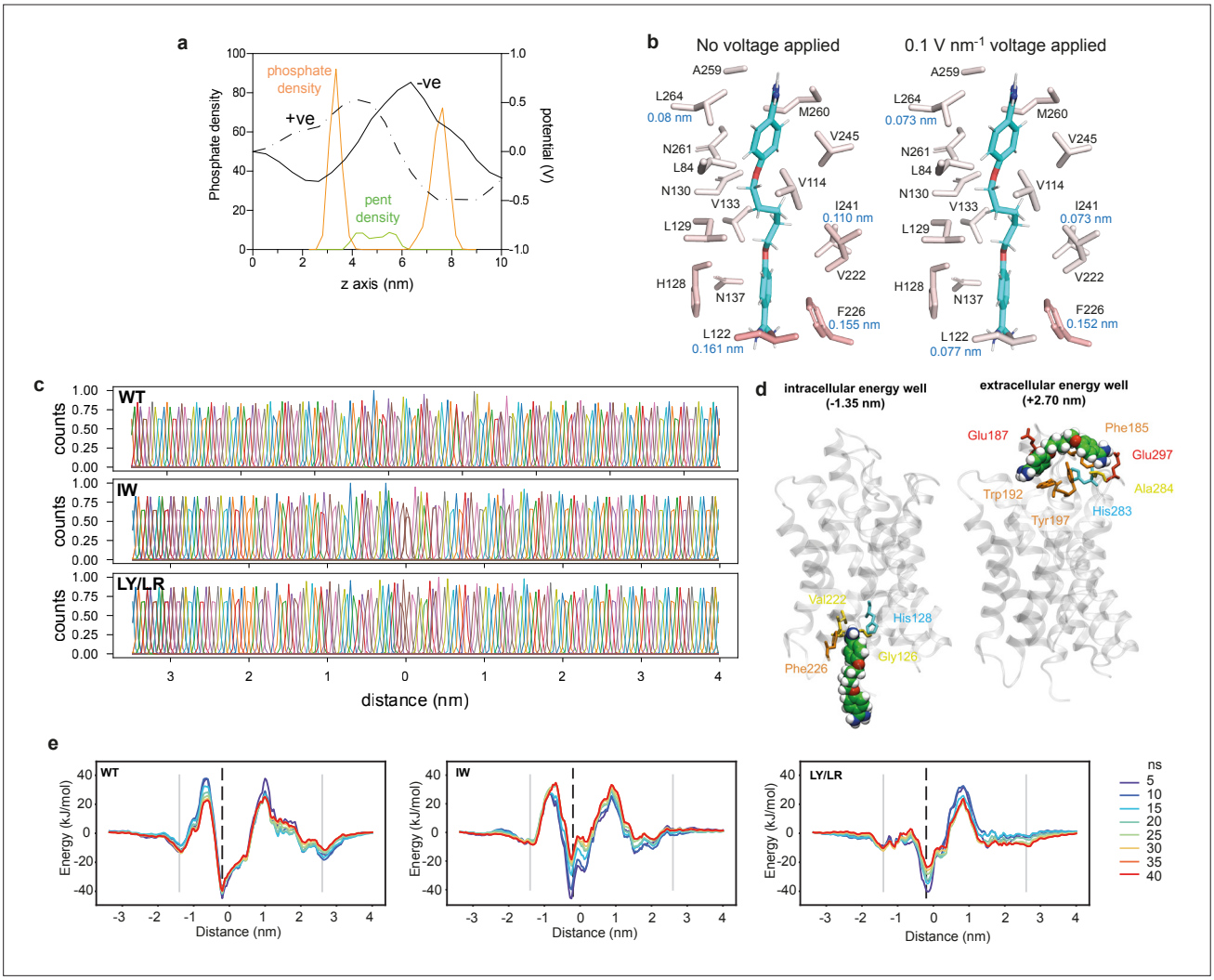


**Figure 5—figure supplement 3.** Molecular dynamics simulations. (**a**) Plot of the membrane potential (V) as applied via an electric field, and calculated using the Gromacs tool *gmx potential*. Shown are potentials produced by an electric field applied in the forward (-ve; solid line) or backward (+ve; dashed line) direction. For context, the densities of lipid phosphate atoms and pent atoms are shown as orange and green traces, as measured using *gmx density*. (**b**) RMSF calculations were run on monomeric TbAQP2 with either no membrane voltage or a 0.1 V $nm^{-1}$ voltage applied (in the physiological direction). Shown are residues in contact with the pentamidine molecule, coloured by RMSF value. RMSF values are shown for residues Leu122, Phe226, Ile241, and Leu264. The data suggest the voltage has little impact on the flexibility or stability of the pore lining residues. (**c**) Histograms for the umbrella sampling simulations used to generate the landscapes in ***Figure 5d***. The data show considerable overlap between windows. (**d**) Snapshots taken from post umbrella sampling windows for WT TbAQP2 at –1.35 nm and +2.7 nm. (**e**) Conversion plots for the PMF landscapes. Shown are landscapes calculated for increasing lengths of simulations (length in ns). After about 30 ns, the landscapes converged.

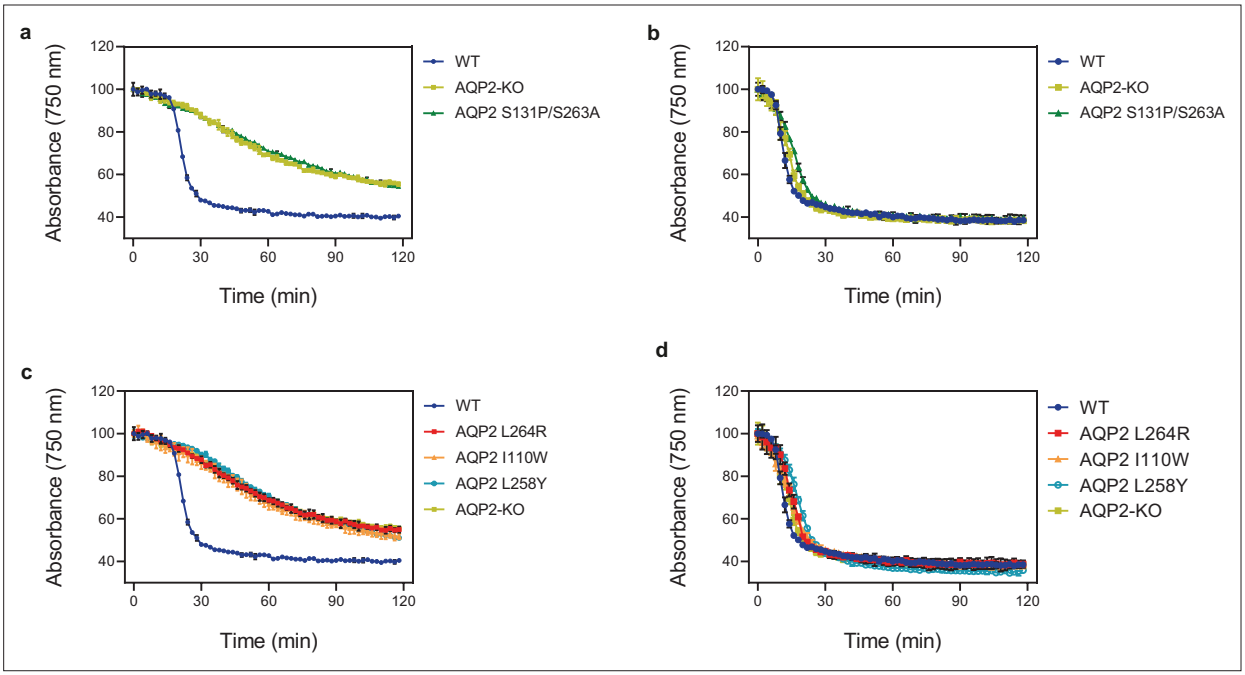


**Figure 6.** Lysis assay of *T. brucei* cells. Lysis assay with *T. b. brucei* wild-type and various AQP2 mutant cell lines treated with arsenical compounds: (**a, c**) cymelarsan; (**b, d**) phenylarsine oxide, a different arsenic-containing trypanocide that enters the parasite independently of TbAQP2 (***Munday et al., 2015b***; ***De Koning, 2001***; ***Munday et al., 2014***) and is thus used as a control for transporter-related arsenic resistance versus resistance to arsenic per se. The cells were placed in a cuvette and treated with either compound at $t$ = 10 min. All points shown are the average of triplicate determinations and SD. When error bars are not visible, they fall within the symbol. The slow decline with cymelarsan over time in AQP2-KO and the mutant cell lines is attributable to residual uptake of the compound through the TbAT1/P2 transporter (***Carter and Fairlamb, 1993***; ***de Koning et al., 2000***).

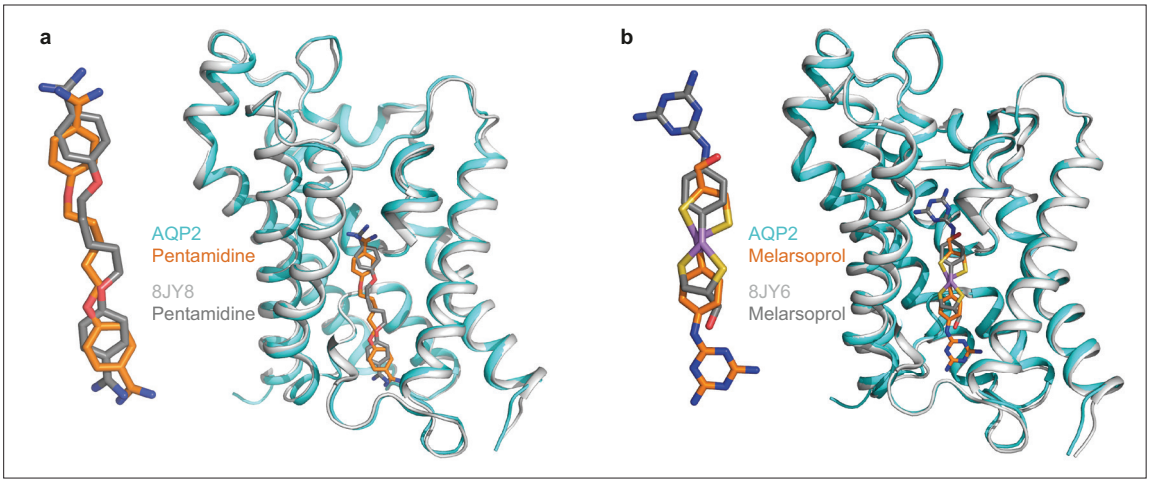


**Figure 7.** Comparison between drug-bound AQP2 structures. Superposition of an AQP2 protomer from this work (cyan) with a protomer determined by ***Chen et al., 2024*** (grey), with the positions of drugs shown in stick representation: (**a**) pentamidine and (**b**) melarsoprol.